Influence of Surface Protonation on the Sensitization Efficiency of Porphyrin-Derivatized TiO_2

David F. Watson, Andras Marton, Arnold M. Stux, and Gerald J. Meyer*

Departments of Chemistry and Materials Science and Engineering, Johns Hopkins University, 3400 North Charles Street, Baltimore, Maryland 21218

Received: April 26, 2004

The influence of electrolyte pH on the sensitization efficiency of porphyrin-derivatized TiO_2 was studied by photoelectrochemical and transient absorption measurements. The porphyrins 5-(4-carboxyphenyl)-10,15,20-trimesitylporphinatozinc(II) (**1**), 5-(4-carboxyphenyl)-10,15,20-trimesitylporphine (**2**), 5-(4-carboxyphenyl)-10,15,20-trimesitylporphinatoplatinum(II) (**3**), and 5-(4-dihydroxyphosphorylphenyl)-10,15,20-trimesitylporphinatozinc(II) (**4**) were anchored to low-surface-area and nanocrystalline TiO_2 films. The TiO_2 conduction band edge potential (E_{CB}) shifted 59 ± 2 mV/pH, from −0.43 V vs $Ag/AgCl_{(aq)}$ at pH 12 to +0.16 V vs $Ag/AgCl_{(aq)}$ at pH 2. Excited-state potentials ($E_{1/2}(P^{+/*})$) of **1**−**4** ranged from −1.58 to −0.91 V vs $Ag/AgCl_{(aq)}$, well negative of E_{CB}. Despite the thermodynamic favorability of electron injection, a 10-fold increase in sensitized photocurrent was measured for **1**−**4** upon acidification of the electrolyte from pH 10 to 4. Transient absorption data revealed that sensitization of nanocrystalline TiO_2 by **1**−**4** depended on pH in an identical manner. A mechanism is proposed wherein protonation of a surface site is required for charge compensation of injected electrons. Thus, the magnitude of sensitized photocurrent is determined by surface protonation-deprotonation equilibria.

Introduction

Dye-sensitized photoelectrochemical cells have been the subject of considerable interest over the past three decades.[1−5] The accepted mechanism for dye-sensitization involves the excitation of a sensitizer followed by interfacial electron transfer, or electron injection, into a semiconductor acceptor state.[1,2,6−8] In regenerative dye-sensitized photoelectrochemical cells, the oxidized sensitizer is reduced by a donor present in the electrolyte, which is in turn reduced at the counter electrode. Thus, photocurrent and photovoltage are generated under sub-bandgap illumination, while no net chemistry occurs. The development of efficient dye-sensitized solar cells using single-crystal electrodes was precluded by poor light harvesting efficiencies and low photocurrent densities. To improve the light harvesting efficiency, Grätzel and co-workers[9−12] developed high surface area, nanocrystalline dye-sensitized metal oxide films. In 1991, O′Regan and Grätzel[13] reported a global power conversion efficiency of ∼7% for a dye-sensitized nanocrystalline TiO_2 electrode under simulated AM 1.5 solar illumination. The efficiency has since been optimized to 10.96%.[14,15]

The cation concentration at the semiconductor-electrolyte interface profoundly influences the efficiency of dye-sensitized photoelectrochemical cells.[16] Cations have been found to affect many parameters, including the energetics of the semiconductor and sensitizer,[17−22] the efficiency and dynamics of electron injection,[23−26] and the kinetics of charge transport.[27,28] Understanding and controlling cation effects is important with regard to maximizing the efficiency of dye-sensitized solar cells.

In the early dye-sensitization literature, several reports described pH-dependent sensitized photocurrents at single-crystal metal oxide electrodes.[29−31] The effect was attributed to the well-known Nernstian dependence of the conduction band edge potential on the electrolyte proton concentration,[17−19] and the resulting pH dependence of the driving force for electron injection. We recently reported pH-dependent sensitized photocurrents for porphyrin-modified, low-surface-area TiO_2 films.[32] This surprising result could not be explained by pH-induced shifts of the TiO_2 conduction band, because electron injection was thermodynamically favorable over the entire pH range through which the photocurrent onset occurred. Instead, the result was attributed to the influence of surface protonation-deprotonation equilibria on the collection efficiency of injected electrons in low-surface-area TiO_2 films.

CHART 1: Structures of the Porphyrin Sensitizers, 1: M = Zn(II), X = CO_2H; 2: M = 2H, X = CO_2H; 3: M = Pt(II), X = CO_2H; 4: M = Zn(II), X = PO_3H_2

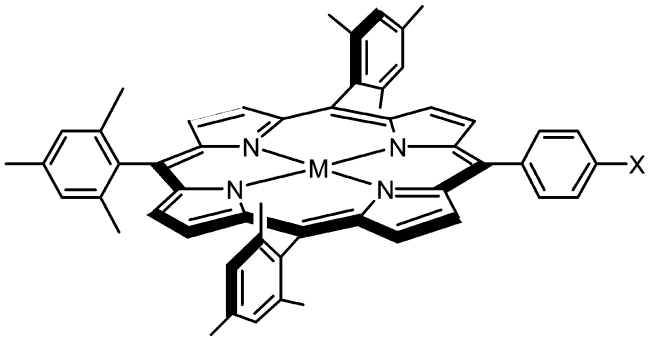

In this manuscript, we report on the continuation of our recent studies. We have characterized the sensitization of nanocrystalline and low-surface-area TiO_2 films with porphyrins **1**−**4** (Chart 1) using photoelectrochemical and spectroscopic techniques. The interfacial proton concentration was found to exert similar effects on the sensitization efficiency of nanocrystalline TiO_2 and low-surface-area TiO_2. Our findings have important implications for optimizing the efficiency of nanocrystalline dye-sensitized photoelectrochemical cells.

10.1021/jp048182x CCC: $27.50
Published on Web 07/01/2004

Experimental Section

Materials. *Porphyrin Synthesis.* Porphyrins **1**, **2**, and **4** were obtained from Prof. J. S. Lindsey's laboratory.[33,34] Porphyrin **3** was synthesized by Pt^{2+} insertion into the free base porphyrin (**2**), following the method of Mink et al.[35]

Semiconductor Film Preparation. Single-crystal rutile TiO_2 (100) was obtained from Princeton Scientific. Crystals were reduced by heating at 600 °C for 1 h in a 10/90 H_2/N_2 atmosphere. Low-surface-area TiO_2 films were prepared by adaptation of the method of Ting et al.[36,37] Elemental Ti was sputter-deposited onto conductive FTO-coated glass slides (8−20 Ω/square, Libby Owens Ford) at room temperature under a 10 mTorr Ar atmosphere at 50 W. Optimal film thickness was achieved with 2−6 min sputtering time. Ti films were oxidized to TiO_2 by heating at 450 °C in air for 30−60 min. Nanocrystalline TiO_2 and ZrO_2 films on glass or FTO substrates were prepared as previously described.[38,39]

Surface Attachment Reactions. TiO_2 films were exposed to solutions of **1**−**4** in toluene or THF for 12−15 h. Upon removal from porphyrin solutions, derivatized slides were rinsed thoroughly with the derivatizing solvent. Surface coverages were determined from the Soret and Q-band absorbances of derivatized films.

Scanning Electron Microscopy. SEM images were obtained with a JEOL scanning electron microscope. Secondary electron images were acquired at 2−10 kV.

Electrochemistry. *Impedance Spectroscopy.* Impedance and capacitance of low-surface-area TiO_2/FTO samples were measured using a Stanford Research SR530 lock-in amplifier (LIA) and a PAR Model 173 potentiostat/galvanostat. All measurements were performed in a three-electrode configuration using a low-surface-area TiO_2/FTO working electrode, Pt mesh counter electrode, and $Ag/AgCl_{(aq)}$ reference electrode. The electrolyte was aqueous 0.1 M $Na_2B_4O_7$, the pH of which was adjusted with HCl and NaOH. The geometry of the electrochemical cell was the same throughout the experiments, enforcing a minimal distance between electrodes and a 0.28 cm^2 working electrode area.

Using a LabView program, the LIA and potentiostat were programmed to obtain frequency vs impedance data and potential vs capacitance data. The LIA was used to generate both the reference signal and the modulating signal (3 mV peak to peak) of known frequency. The modulating signal was added onto the potential generated by the potentiostat. The current to voltage output of the potentiostat was connected to the voltage input of the LIA. The LIA was then used to measure the real and imaginary part of the current in the electrochemical cell as a function of either frequency or potential. The real and imaginary impedance (Z) and capacitance (C) were calculated by the program. Complex plane plots of the impedance ($|\mathrm{Im}(Z)|$ vs $\mathrm{Re}(Z)$), Bode plots ($\log(|Z|)$ vs $\log(\omega)$), and C vs potential plots were also produced by the LabView program.

Photocurrent Onset Potentials. Band gap photocurrents were measured in a 3-electrode, single compartment cell with a low-surface-area TiO_2/FTO working electrode, Pt-coated FTO counter electrode, and $Ag/AgCl_{(aq)}$ reference electrode. The electrolyte was aqueous 0.1 M $Na_2B_4O_7$, the pH of which was adjusted with HCl and NaOH. Linear sweep voltammograms ($V = 10$ mV/s) were measured in the dark and under chopped (320 Hz) illumination by the full spectral output of a Xe lamp. Photocurrents were measured by lock-in technique with a Stanford Research Systems SR530 lock-in amplifier.

Cyclic Voltammetry. Cyclic voltammetry was performed with a Bioanalytical Systems CV-50 potentiostat. A 3-electrode, single-compartment cell was used, with a porphyrin-derivatized TiO_2 working electrode, Pt mesh counter electrode, and $Ag/AgCl_{(aq)}$ reference electrode. The electrolyte was 0.1 M tetrabutylammonium perchlorate in CH_3CN or 0.1 M $Na_2B_4O_7$ in water. The pH of the aqueous electrolyte was adjusted with HCl and NaOH.

Sensitized Photocurrent Measurement. Photocurrents were measured using one of two setups. (1) A 3-electrode sandwich cell was employed, with a porphyrin-modified TiO_2/FTO working electrode, Pt-coated FTO counter electrode, and Ag pseudoreference electrode. The electrolyte was 0.1 M aqueous $Na_2B_4O_7$ with 0.05 M hydroquinone as an electron donor. The electrolyte pH was adjusted with HCl and NaOH. The working electrode was illuminated through the backside using a Schoeffel CPS 255HR 450 W Xe lamp coupled to a Kratos GM252 monochromator. Current was measured with a PAR 173 potentiostat output to a Houston Instruments 2000 X−Y recorder. Photocurrent action spectra were measured at constant positive bias at potentials corresponding to saturation sensitized photocurrent, as determined from linear sweep voltammetry measurements under chopped (∼1 Hz) Soret band illumination. (In linear sweep experiments, potential was controlled with a PAR 175 universal programmer.) (2) A 2-electrode sandwich cell was employed, with a porphyrin-modified TiO_2/FTO working electrode and Pt-coated FTO counter electrode. The working electrode was illuminated through the backside using a 150 W Spectra-Physics Xe lamp coupled to an Oriel Cornerstone 1/4*m* monochromator. Current was measured by a Keithley 617 electrometer.

Spectroscopy. *Static Absorption and Emission.* UV/vis absorption spectra were obtained with a Hewlett-Packard 8453 diode array spectrophotometer. Emission spectra were obtained with a Spex Fluorolog fluorimeter. Porphyrin-modified films were placed diagonally in a 1 cm cuvette, and front-face emission was measured.

Transient Absorption Spectroscopy. Transient absorption data were acquired as described previously.[24] The frequency-tripled, 355 nm output of a Q-switched Nd:YAG laser (Continuum Surelite) was Raman-shifted with $H_{2(g)}$, yielding pulsed 417 nm irradiation (∼8 ns, 5−10 mJ/cm^2, 1 Hz). Sensitizer-derivatized semiconductor films were placed in a 1-cm quartz cuvette at a 45° angle to the pump beam. The cuvette was stoppered, and the surrounding aqueous electrolyte solution was purged with Ar or N_2. The pump beam was expanded to an ∼1.5-cm diameter to ensure uniform illumination of the sensitizer-derivatized films. The probe source was a pulsed 150 W Xe lamp (Applied Photophysics) focused on the semiconductor film. Transmitted light was output through a Spex 1702−04 monochromator and detected with a Hamamatsu R928 PMT. The pump and probe beams were orthogonal. The PMT signal was digitized by a LeCroy 9450 oscilloscope.

Results

TiO_2 Morphology. Two types of TiO_2 film were prepared: "low-surface-area" films from thermal oxidation of sputter-deposited titanium, and nanocrystalline films from sol−gel deposition. Scanning electron micrographs of low-surface-area TiO_2 films (Figures 1a-c) reveal that the morphology of the films depended on the sputter deposition time scale. At short deposition times (≤4 min), the TiO_2 films consisted of relatively large particles with dimensions on the order of 100 nm. Some additional surface roughness on the individual TiO_2 particles is apparent. The morphology of these films corresponded closely to that of their FTO substrates. Increasing the sputter deposition

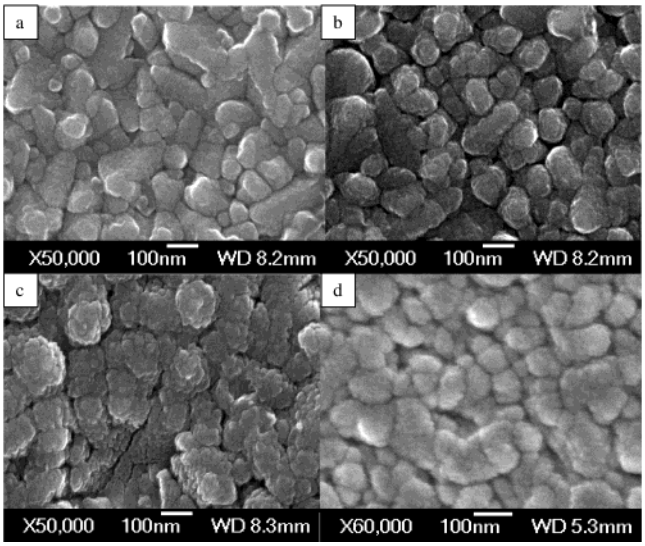

Figure 1. Scanning electron micrographs of TiO_2 films on FTO. Images a−c are low-surface-area TiO_2 films prepared by oxidation of sputter-deposited titanium films at deposition times of 4 min (a), 7.5 min (b), and 30 min (c). Image d is a nanocrystalline film from the sol−gel preparation.

time resulted in increased film thickness and increased surface area through the formation of smaller TiO_2 particles. The film prepared by oxidation of 30-minute sputtered titanium consisted of aggregates of TiO_2 with features on an approximately 10-nm length scale. The nanocrystalline TiO_2 film also consisted of aggregates of particles with roughly 10-nm dimensions (Figure 1d).

Sensitizer Adsorption. Porphyrins **1**−**4** were adsorbed to TiO_2 surfaces from solution. Equilibrium binding was well-described by the Langmuir adsorption isotherm model (Figure 2).[40] Porphyrins were adsorbed to low-surface-area TiO_2 films (2−6 min sputter deposition time) with surface adduct formation constants (K_{ad}) of 10^5 M^{-1} and saturation surface coverages (Γ_{max}) of 4.0×10^{-10} mol/cm^2. For nanocrystalline TiO_2 films, $K_{ad} = 10^4$ M^{-1} and $\Gamma_{max} = 9.7 \times 10^{-8}$ mol/cm^2.

Attempts to adsorb the tetramesityl analogue of **1** to TiO_2 yielded no measurable surface coverage, suggesting that **1**−**4** are anchored to the surface through carboxylic acid or phosphonic acid functional groups. When low-surface-area TiO_2 films derivatized with **1**, **2**, or **3** were immersed in organic solvents in which the porphyrins were soluble, rapid and nearly complete desorption occurred. Low-surface-area TiO_2 derivatized with **4**, which contains the phosphonic acid surface-attachment group, underwent little or no desorption in organic solvents. For all four porphyrins, very little desorption occurred from nanocrystalline TiO_2 films immersed in organic solvents.

Porphyrins **1**−**4** remained attached to low-surface-area TiO_2 when the films were immersed in water. The stable surface attachment is attributed to the insolubility of the porphyrins in water. The absorption spectra of porphyrin-derivatized TiO_2 films immersed in aqueous solution were independent of pH, indicating that the porphyrins were stable toward diacid formation.[41,42] The absorption and emission spectra of surface-attached porphyrins were minimally perturbed from their solution spectra. The absorption and emission spectra of **1** and **4**, which differ in the nature of the surface-attachment group, were superimposable. These observations suggest that electronic coupling is relatively weak through the phenylene spacer connecting the porphyrin ring and the surface-attachment group.

Semiconductor Energetics. The flat-band potentials (E_{FB}) of underivatized, low-surface-area TiO_2 films were determined from Mott−Schottky analysis of impedance spectroscopy data (Figure 3a) and from the onset potentials of band gap photocurrent.[19,43,44] Flat-band potentials determined from both methods were in close agreement (Figure 3b). Therefore, significant band-edge unpinning does not occur under illumination. Mott−Schottky plots ($1/C_p^2$ vs V) were obtained at 10 and 100 Hz, which fall within the capacitive regime of the Bode plot at each electrolyte pH. The conduction band edge potential (E_{CB}) was estimated from E_{FB}:

$$E_{CB} = E_{FB} - k_B T \ln\left(\frac{n_D}{N_C}\right) \quad (1)$$

where n_D is the donor density and N_C is the density of states at the conduction band edge.[30,45,46] Donor densities of 10^{18} cm^{-3} were calculated from Mott−Schottky slopes. Assuming that $N_C \sim 10^{20}$ cm^{-3}, E_{CB} is no more than 120 mV negative of E_{FB}.

E_{FB} values derived from Mott−Schottky plots shifted linearly with pH, with the expected Nernstian slope of 59 ± 2 mV/pH. From pH 2 to 12, E_{FB} varied from +0.16 to −0.43 V vs Ag/$AgCl_{(aq)}$. Impedance experiments were performed on **4**-modified low-surface-area TiO_2 at pH 10 and pH 12. (At more acidic pH's, porphyrin oxidation current prevented impedance measurement.) E_{FB} values of **4**-modified TiO_2 films were within 100 mV of those of unmodified TiO_2.

Sensitizer Energetics. Porphyrin ground-state reduction potentials ($E_{1/2}(P^{+/0})$) were determined by cyclic voltammetry. Porphyrins **1** and **4**, adsorbed to low-surface-area TiO_2, underwent reversible one-electron ring oxidation. At pH 1, the $E_{1/2}(P^{+/0})$ values of **1** and **4** were +0.71 and +0.68 V vs Ag/AgCl. The $E_{1/2}(P^{+/0})$ values of **1** and **4** were weakly pH-dependent, shifting 15 ± 6 mV/pH and 10 ± 1 mV/pH, respectively. These shifts are consistent with previously reported measurements on phthalocyanine dyes attached to nanocrystalline TiO_2.[47] Reversible one-electron oxidation was observed for **1** adsorbed to nanocrystalline TiO_2, with identical $E_{1/2}(P^{+/0})$ values as on low-surface-area TiO_2. The $E_{1/2}(P^{+/0})$ values of **2** and **3** were more positive than the $E_{1/2}(P^{+/0})$ values of **1** and **4**, and were outside the aqueous solvent window. In acetonitrile electrolyte, **2** adsorbed to low-surface-area TiO_2 underwent quasireversible one-electron oxidation with $E_{1/2}(P^{+/0}) = +1.09$ V vs Ag/AgCl. TiO_2-adsorbed **3** underwent irreversible one-electron oxidation with $E_{ox} = +1.16$ V vs Ag/AgCl. An $E_{1/2}(P^{+/0})$ value of +1.08 V vs Ag/AgCl was estimated by assuming a similar peak-to-peak separation as observed for **3**. The measured $E_{1/2}(P^{+/0})$ value of TiO_2-adsorbed **3** is roughly 100 mV positive of reported values for Pt(II) tetraphenylporphyrin in solution.[35,48]

The excited-state reduction potentials ($E_{1/2}(P^{+/*})$) of surface-bound porphyrins were calculated using the standard Rehm−Weller equation,[49] where E_{00} values were estimated from the emission spectra of porphyrins bound to nanocrystalline ZrO_2 films. The emission spectra of porphyrin-modified ZrO_2 films immersed in aqueous solution were pH-independent. The $E_{1/2}(P^{+/*})$ values of **1**−**4** span a range of 670 mV. The potential difference between $E_{1/2}(P^{+/*})$ and E_{CB} determines the thermodynamic favorability of electron injection. For all four porphyrins, $E_{1/2}(P^{+/*})$ is more than 450 mV more negative of E_{CB}, even at the most basic pH's where E_{CB} is most negative. Sensitizer energetics are summarized in Table 1.

Photoelectrochemistry. Anodic photocurrents were measured for porphyrin-modified, low-surface-area TiO_2 electrodes. Photocurrent action spectra (Figure 4) agreed with absorptance spectra. The magnitude of sensitized photocurrent increased by about

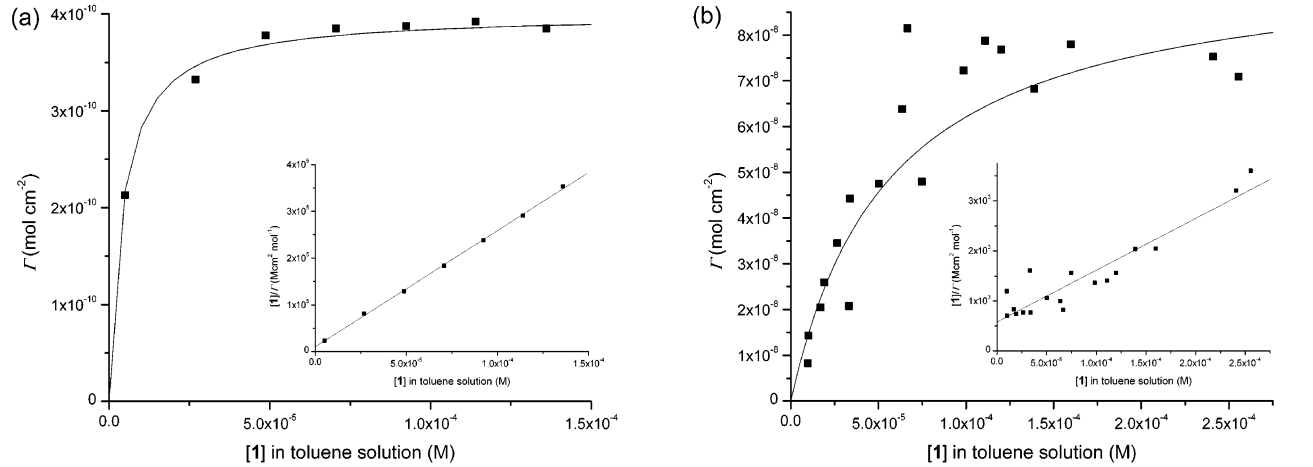

Figure 2. Equilibrium binding data for **1** on low-surface-area TiO_2 (a) and nanocrystalline TiO_2 (b). The insets show plots of [**1**]/Γ vs [**1**] and fits to the Langmuir adsorption isotherm. For low-surface-area TiO_2, $K_{ad} = 10^5\ M^{-1}$ and $\Gamma_{max} = 4.0 \times 10^{-10}$ mol/cm^2. For nanocrystalline TiO_2, $K_{ad} = 10^4\ M^{-1}$ and $\Gamma_{max} = 9.7 \times 10^{-8}$ mol/cm^2. Superimposed on the plots of Γ vs concentration are fits to the data based on the calculated values of K_{ad} and Γ_{max}.

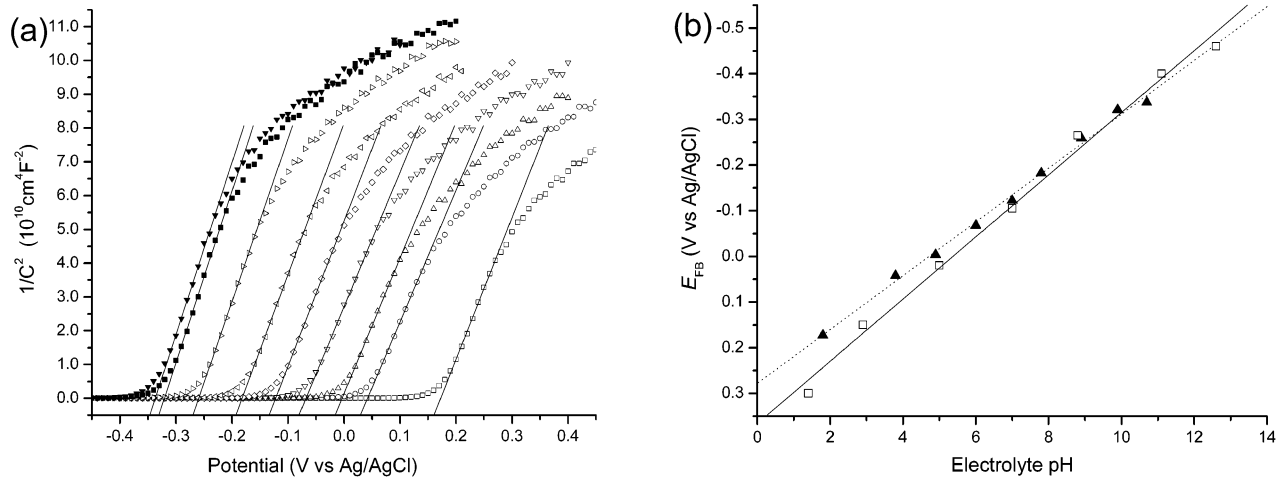

Figure 3. (a) Mott−Schottky plots for an underivatized low-surface-area TiO_2 film with frequency of 100 Hz and peak to peak voltage oscillation of 3 mV. Electrolyte pH = 1.8 (□), 3.8 (○), 4.9 (△), 6.0 (▽), 7.0 (◊), 7.8 (left-facing triangle), 8.9 (right-facing triangle), 9.9 (■), and 10.7 (▼). Superimposed are linear fits of the data. (b) TiO_2 flat-band potential (E_{FB}) vs electrolyte pH for an underivatized low-surface-area TiO_2 film. E_{FB} was estimated from the onset potentials of band gap photocurrent (□, slope = 68 ± 3 mV/pH) and from the *x*-intercepts of Mott−Schottky plots (▲, slope = 59 ± 2 mV/pH).

TABLE 1: Energetics of Surface-Bound Porphyrins

porphyrin	$E_{1/2}(P^{+/0})$ (V)[a,b]	E_{00} (eV)	$E_{1/2}(P^{+/*})$ (V)[a,b]	$\lvert E_{1/2}(P^{+/*}) - E_{CB}\rvert$, pH 12 (eV)[c,d]
1	+0.54	2.11	−1.57	1.14
2	+1.09	2.10	−1.01	0.58
3	+1.08	1.99	−0.91	0.48
4	+0.57	2.15	−1.58	1.15

[a] For **1** and **4**, pH 12 data are reported. [b] Potentials are reported vs Ag/AgCl. [c] E_{CB} of low-surface-area TiO_2 at pH 12 = −0.43 V vs Ag/AgCl. [d] $\lvert E_{1/2}(P^{+/*}) - E_{CB}\rvert$ indicates the thermodynamic favorability of electron injection, and is lowest at basic pH's where E_{CB} is most negative.

10-fold at pH < 5, independent of which porphyrin was used. Plots of photocurrent vs pH for **1**−**4** were nearly identical, despite the 670 mV range in $E_{1/2}(P^{+/*})$ values (Figure 4a, inset). The data were independent of whether surface-attachment was through the carboxylic acid or phosphonic acid surface attachment group. No changes were observed in the absorption spectra or photoaction spectra of porphyrin-derivatized TiO_2 electrodes following photoelectrochemical measurements. The observed proton dependencies were reversible and independent of hydroquinone donor concentration. The decrease in photocurrent at basic pH's cannot be attributed to decreased hydroquinone oxidation kinetics, because hydroquinone oxidation is more favorable at high pH.[50] Control experiments using porphyrin-modified single-crystal TiO_2 or using iodide as the electron donor revealed the same pH dependence. Attempts to measure the pH dependence of sensitized photocurrent for porphyrin-modified nanocrystalline TiO_2 films were complicated by the observation of cathodic sensitized photocurrents at acidic pH.

Short-circuit photocurrents (i_{sc}) were linear with respect to incident photon flux (PF), and open-circuit photovoltages (V_{oc}) were linear with respect to log(PF). V_{oc} increased 65−100 mV per decade increase of PF, corresponding to an "ideality factor" of 1.1 to 1.7.[51] With hydroquinone as the electron donor species, V_{oc} was independent of pH in acidic electrolytes (pH < 5) where maximum sensitized photocurrents were measured.

Transient Absorption Spectroscopy. Transient absorption data were obtained for **1**-modified nanocrystalline TiO_2 and ZrO_2 films immersed in 0.1 M $Na_2B_4O_7$ at pH 2.1, with excitation into the Soret band at 417 nm (Figure 5). The surface coverage (Γ) of **1** was 3×10^{-9} mol/cm^2 on both TiO_2 and ZrO_2. Transient absorbance difference spectra decayed with wavelength-independent kinetics. The spectrum of **1** on ZrO_2

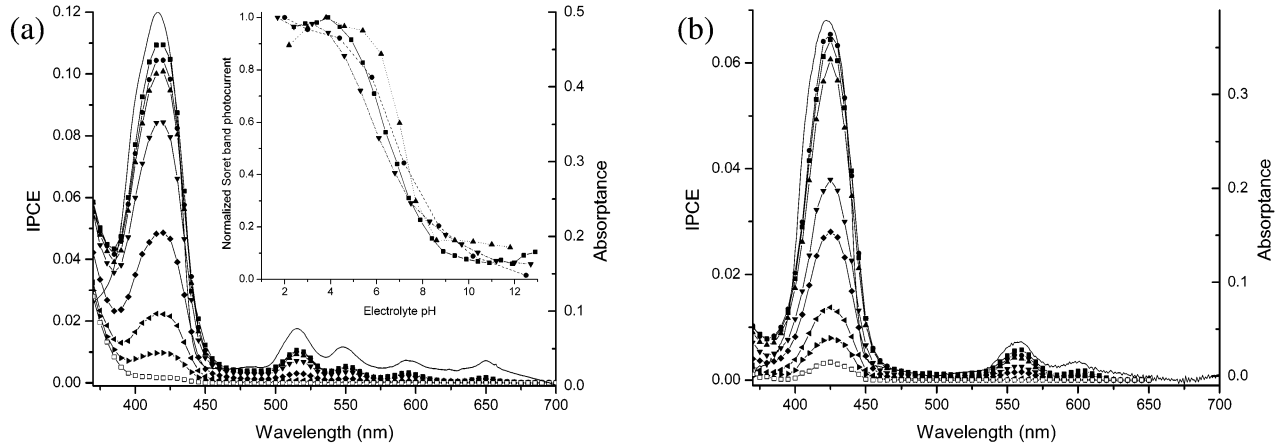

Figure 4. (a) Photocurrent action spectra of **2**-derivatized low-surface-area TiO_2 film at electrolyte pH's of 2.0 (■), 3.0 (●), 4.4 (▲), 5.8 (▼), 7.2 (♦), 8.7 (left-facing triangle), 10.2 (right-facing triangle), and 12.5 (□). (b) Photocurrent action spectra of **1**-derivatized low-surface-area TiO_2 film at electrolyte pH's of 2.0 (■), 3.5 (●), 5.0 (▲), 6.5 (▼), 8.0 (♦), 9.5 (left-facing triangle), 11.0 (right-facing triangle), and 12.5 (□). IPCE = incident photon-to-current efficiency. Superimposed on the photoaction spectra are absorptance spectra of the films (−). *Inset to Figure 4a:* Plots of Soret band photocurrent vs electrolyte pH for **1**(■), **2**(●), **3**(▲), and **4**(▼).

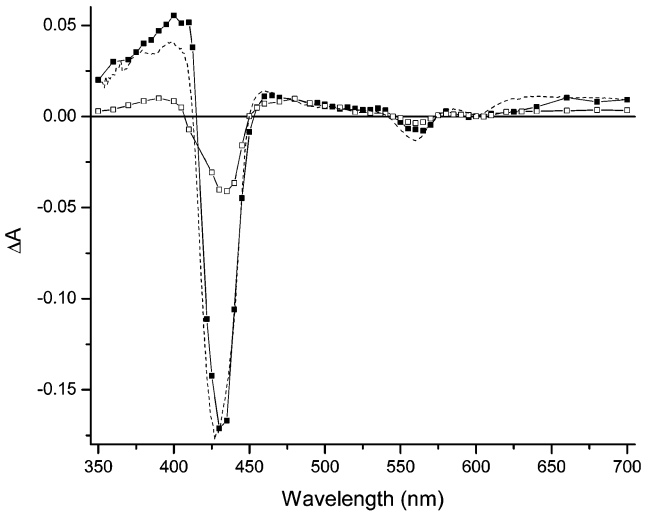

Figure 5. Transient absorbance difference (ΔA) spectra of **1**-modified nanocrystalline TiO_2 (■) and **1**-modified nanocrystalline ZrO_2 (□) films, 10 ns after 417 nm excitation. $\Gamma_1 = 3 \times 10^{-9}$ mol/cm^2 on both films. The films were immersed in 0.1 M $Na_2B_4O_7$ at pH 2.1. Superimposed on the spectrum of **1**-modified TiO_2 is a simulated spectrum (---) based on the sum of contributions from the $^3(\pi,\pi^*)$ excited state and the oxidized porphyrin.

consists of a broad absorption band overlapping the bleach of the ground-state Soret band, and a weaker absorption overlapping the $Q(1,0)$ bleach. The spectrum is assigned to the $^3(\pi,\pi^*)$ excited-state, herein referred to as **1***. The $^1(\pi,\pi^*)$ excited-state lifetimes of Zn(II) tetraarylporphyrins are <10 ns, which is faster than the temporal resolution of our instrument.[52] Electron injection is precluded on ZrO_2, so the formation of oxidized porphyrin under Soret band excitation is not expected.[24] The spectrum of **1*** on ZrO_2 is similar to the $^3(\pi,\pi^*)$ excited-state spectrum of Zn(II) tetraphenylporphyrin (ZnTPP) in solution.[52,53] The excited-state absorption band from 370 to 525 nm is slightly blue-shifted relative to the corresponding band for ZnTPP in solution. The spectrum of **1*** in toluene solution (not shown) was nearly identical to the solution spectrum of the $^3(\pi,\pi^*)$ excited-state of ZnTPP.

The transient absorbance difference spectrum of TiO_2-**1** differs in several respects from the spectrum of ZrO_2-**1**. The transient absorption band in the Soret region is blue-shifted and significantly more intense for **1** on TiO_2 than on ZrO_2. In addition, the Soret band bleach at 430 nm and the absorption from 625 to 700 nm are more intense in the data for **1** on TiO_2. These changes are consistent with oxidation of **1** to yield the π-cation radical (**1**$^{+\bullet}$) as a result of electron injection into TiO_2. The absorption spectrum of **1**$^{+\bullet}$ was measured in a spectroelectrochemical experiment by biasing a **1**-modified nanocrystalline TiO_2 film on FTO at +0.9 V vs Ag/AgCl. The absorption spectrum of **1**$^{+\bullet}$ on TiO_2 corresponded closely with the spectrum of ZnTPP$^{+\bullet}$ in solution.[54] The absorption band in the Soret region for **1**$^{+\bullet}$ is blue-shifted and narrow compared with the corresponding band for **1***. The absorbance from 625 to 700 nm is greater in the spectrum of **1**$^{+\bullet}$ than in the spectrum of **1***. The transient absorbance difference spectrum of **1**-modified TiO_2 was accurately simulated as the sum of contributions from the spectra of **1**$^{+\bullet}$ and **1*** (Figure 5). By assuming that the extinction coefficients of **1**$^{+\bullet}$ and **1*** are equal to the corresponding values for ZnTPP$^{+\bullet}$ and ZnTPP*,[52−54] the ratio of **1**$^{+\bullet}$ to **1*** on TiO_2 was estimated from the simulation to be ∼8:1.

Three transient spectral features are useful for distinguishing between **1**$^{+\bullet}$ and **1***: (a) the amplitude of the absorption from 350 to 400 nm, (b) the amplitude of the ground-state Soret band bleach, and (c) the amplitude of the absorption from 650 to 700 nm. Transient absorption data were acquired for a **1**-modified nanocrystalline TiO_2 film immersed in 0.1 M $Na_2B_4O_7$ as a function of the electrolyte pH. Data were collected at 380, 430, and 700 nm, where the extinction coefficients of **1**$^{+\bullet}$ and **1*** are significantly different. The absorbances at 380 and 700 nm decreased with increasing pH (Figure 6a,c). Similarly, the amplitude of the bleach at 430 nm decreased with increasing pH (Figure 6b). These trends were reversible and independent of the surface coverage of **1**. The concentration of **1**$^{+\bullet}$ on the TiO_2 surface at delay times ≥ 10 ns after Soret band excitation increased 10-fold with acidification of the surrounding aqueous solution from pH 10 to 2. Plots of the normalized absorbance difference ($\Delta A_0/\Delta A_{0,max}$) vs pH for **1**-modified nanocrystalline TiO_2 overlaid precisely with the plot of sensitized photocurrent vs electrolyte pH for **1**-modified low-surface-area TiO_2 (Figure 7).

Discussion

The saturation surface coverage (Γ_{max}) reflects the total number of porphyrin binding sites on the TiO_2 surface. Therefore, the equilibrium binding data indicate that the surface roughness of nanocrystalline TiO_2 films is approximately 250 times greater than that of the low-surface-area TiO_2 films. The

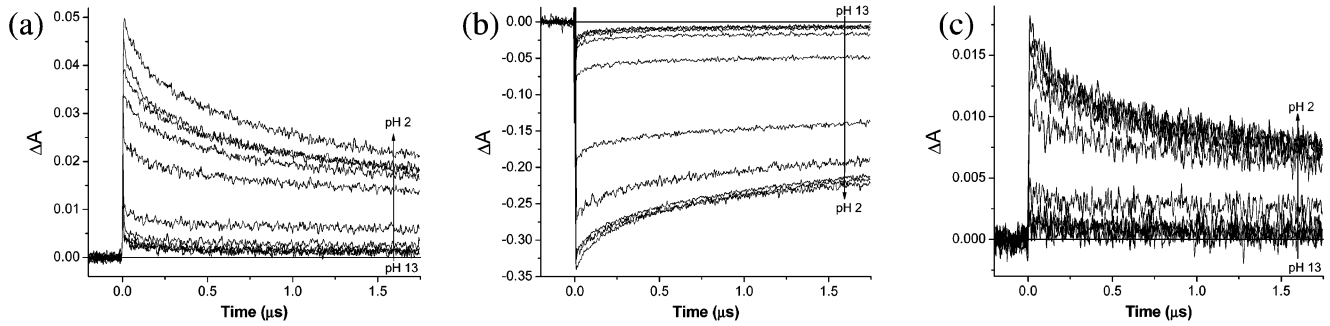

Figure 6. Transient absorbance difference (ΔA) traces at 380 nm (a), 430 nm (b), and 700 nm (c) for a **1**-modified nanocrystalline TiO_2 film immersed in 0.1 M $Na_2B_4O_7$ at pH's of 2.1, 3.3, 4.4, 5.6, 6.6, 7.7, 9.0, 10.2, 11.7, and 13.2. The pump wavelength was 417 nm.

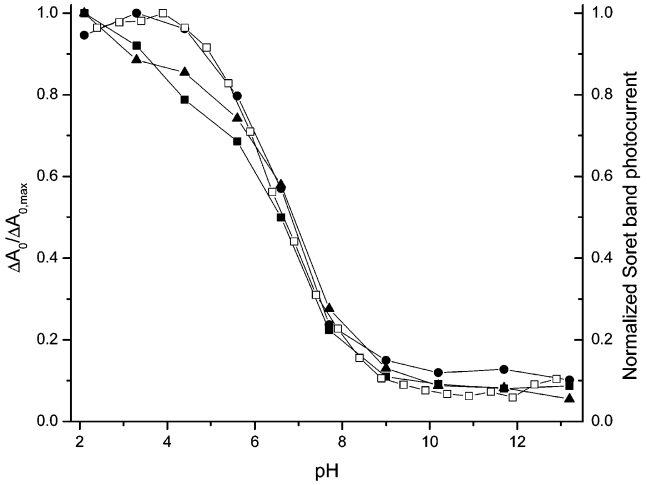

Figure 7. pH Dependence of the normalized absorbance difference ($\Delta A_0/\Delta A_{0,max}$), 10 ns after pulsed laser excitation, at 380 nm (■), 430 nm (●), and 700 nm(▲) for a **1**-modified nanocrystalline TiO_2 film. Superimposed on the data is the pH dependence of Soret-band sensitized photocurrent for a **1**-modified low-surface-area TiO_2 film (□).

SEM images of nanocrystalline TiO_2 and low-surface-area TiO_2 from oxidation of 30-minute sputtered titanium are nearly indistinguishable, indicating that the surface morphologies are similar (Figure 1c,d). These observations suggest that the TiO_2 films prepared by oxidation of sputter-deposited titanium are accurately characterized as thin, low-surface-area analogues of nanocrystalline TiO_2 films.

Determining the flat-band potential (E_{FB}) of nanocrystalline TiO_2 films from capacitance measurements is not straightforward, because semiconductor particles of 10−20 nm in diameter cannot support a significant space charge layer.[5,21,55,56] The low-surface-area TiO_2 films are useful analogues of nanocrystalline films, as E_{FB} was readily determined by Mott−Schottky analysis of capacitance data. The observed 59 ± 2 mV/pH shift of E_{FB} for low-surface-area TiO_2 films is consistent with previously reported measurements for single-crystal metal oxides.[17−19,30,57,58] The Nernstian shift of E_{FB} is attributed to the influence of protonation-deprotonation equilibria on the surface charge and the potential drop across the Helmholtz layer, which determines the band edge potentials. A wide range of E_{FB} values has been reported for single-crystal TiO_2, spanning more than 600 mV at a given pH.[17] The measured E_{FB} values for low-surface-area TiO_2 fall within this range.

Photocurrent and transient absorption data were strongly pH-dependent. As detailed in the Results section, the amplitudes of the transient absorbance at 380, 430, and 700 nm are proportional to the concentration of $\mathbf{1}^{+\bullet}$ on the TiO_2 surface. The formation of $\mathbf{1}^{+\bullet}$ on the TiO_2 surface is attributed to electron injection. Therefore, the normalized transient absorbance at these wavelengths must also be proportional to the concentration of electrons in TiO_2. Plots of $\Delta A_0/\Delta A_{0,max}$ vs pH for **1**-modified nanocrystalline TiO_2 were coincident with plots of sensitized photocurrent vs pH for porphyrin-modified low-surface-area TiO_2. Thus, the concentration of $\mathbf{1}^{+\bullet}$ on the nanocrystalline TiO_2 surface and the concentration of electrons in TiO_2, at delay times ≥ 10 ns after porphyrin excitation, exhibit the same pH dependence as the sensitized photocurrent of porphyrin-derivatized low-surface-area TiO_2.

The pH dependence of photocurrent and transient absorption data could arise from pH-induced changes in the absorptance (α), electron injection yield (ϕ_{inj}), or charge collection efficiency (η_{el}). The incident photon-to-current efficiency (*IPCE*) is proportional to the magnitude of sensitized photocurrent, and equals the product of α, ϕ_{inj}, and η_{el}:[4,5]

$$IPCE = \alpha \times \phi_{inj} \times \eta_{el} \tag{2}$$

Similarly, the concentration of electrons in TiO_2 following electron injection ($[e^-]_{sc}$) must depend on α, ϕ_{inj}, and the charge recombination efficiency (η_{cr}), where $\eta_{cr} = 1 - \eta_{el}$:

$$[e^-]_{sc} \propto \alpha \times \phi_{inj} \times (1 - \eta_{cr}) \tag{3}$$

The absorption spectra of porphyrin-derivatized low-surface-area and nanocrystalline TiO_2 films immersed in aqueous solution were invariant with changes in pH, indicating that α is pH-independent. Therefore, either the electron injection yield or the charge collection efficiency must be pH-dependent.

We first consider the possibility that the electron injection yield is pH-dependent. According to the accepted mechanism of anodic sensitization, the rate of electron injection (k_{inj}), and therefore the injection yield, is proportional to the overlap of occupied sensitizer excited-states and unoccupied semiconductor acceptor states:

$$k_{inj} \propto \int \kappa(E) D(E) W_{don}(E) \mathrm{d}E \tag{4}$$

where $\kappa(E)$ is the transfer frequency, $D(E)$ is the density of unoccupied acceptor states in the semiconductor, and $W_{don}(E)$ is the sensitizer excited-state distribution function.[1,6] $W_{don}(E)$ has been expressed as follows:

$$W_{don}(E) = \frac{1}{\sqrt{4\pi\lambda k_B T}} \exp\left(-\frac{(E - E_{1/2}(S^{+/*}) + \lambda)^2}{4\lambda k_B T}\right) \tag{5}$$

where E is potential, $E_{1/2}(S^{+/*})$ is the sensitizer excited-state potential, and λ is the reorganization energy of electron injection.[1,30,31,59] The density of unoccupied conduction band states should increase with the square root of energy above

E_{CB}.[30] Therefore, k_{inj} should be maximized when $[E_{1/2}(P^{+/*}) + 2\lambda] < E_{CB}$, or when the entire excited-state distribution function lies at a more negative potential than E_{CB}. In previous studies, the pH dependence of sensitized photocurrent was attributed to changes in ϕ_{inj}, as a result of changes in the degree of overlap between $W_{don}(E)$ and $D(E)$ caused by pH-induced movement of E_{CB}.[29-31] The width of $W_{don}(E)$ was determined from the pH range through which the photocurrent increased to its maximum. Values of λ were determined to be ≤ 375 mV.[30,31]

We considered a similar analysis of the pH-dependent photoelectrochemical and spectroscopic data for porphyrin-derivatized TiO_2. The onset of sensitized photocurrents for **1**−**4** occurred from pH 10 to pH 4. If the pH dependence of photocurrent arose from changes in ϕ_{inj}, due to positive shifts of E_{CB} with decreasing pH, then the data would imply that $2\lambda = 6(59$ mV/pH), or $\lambda = 177$ mV. However, this interpretation is inconsistent with the observation that the photocurrent onset was independent of which sensitizer was used. That is, if ϕ_{inj} were pH-dependent, the maximum sensitized photocurrents would occur at pH's where $[E_{1/2}(P^{+/*}) + 2\lambda] < E_{CB}$. At pH 4, the $E_{1/2}(P^{+/*})$ values of **1**−**4** range from 0.79 to 1.54 V negative of E_{CB}, which would imply that λ should range from 395 mV to 770 mV. Such high reorganization energies are inconsistent with the 6 pH-unit range through which the photocurrent onsets occurred. (In addition, a reorganization energy of 770 mV would be unprecedented and would imply an extraordinarily broad excited-state distribution function.) Expressed differently, if ϕ_{inj} varied with pH and λ was approximately equal for **1**−**4**, we would expect plots of photocurrent vs pH for the different porphyrins to be displaced along the pH axis. For example, because $E_{1/2}(P^{+/*})$ of **2** is 560 mV more positive than $E_{1/2}(P^{+/*})$ of **1**, the photocurrent vs pH plot for **2** would be shifted 9.5 pH units more acidic than the plot for **1**. Similarly, the photocurrent vs pH plot for **3** would be shifted 11.4 pH units more acidic than that of **4**. Clearly, these shifts were not observed.

Clark and Sutin[30] also observed pH-dependent sensitized photocurrents under conditions where E_{CB} was far positive relative to the sensitizer excited-state potential, and the injection yield should have been pH-independent. The maximum photocurrents were observed at pH's where the measured value of E_{CB} was roughly 850 mV positive of the sensitizer excited-state potential. Clark and Sutin considered five possible explanations for the discrepancy between the predicted and observed pH ranges of photocurrent onset: (1) inaccurate measurement of $E_{1/2}(S^{+/*})$; (2) inaccurate measurement of E_{CB}; (3) band-edge unpinning under applied bias; (4) shifts of E_{CB} due to sensitizer adsorption; and (5) underestimation of N_C, the density of states at the conduction band edge, resulting in inaccurate calculation of the difference between E_{FB} and E_{CB}. They proposed that the underestimation of N_C was most likely.

In the case of porphyrin-modified TiO_2, none of the five possibilities seems likely. The $E_{1/2}(P^{+/*})$ values of TiO_2-adsorbed **1**−**4** were accurately measured from cyclic voltammetry and emission measurements, and corresponded well with solution values and with previously reported values for similar porphyrins.[35,48,60,61] The E_{CB} values determined by Mott−Schottky analysis and photocurrent onset measurements were in close agreement, implying minimal band-edge unpinning (Fermi level pinning) under applied bias or under illumination. Mott−Schottky data for **4**-derivatized low-surface-area TiO_2 corresponded closely with data for underivatized TiO_2, indicating that sensitizer adsorption does not significantly influence E_{CB}. The underestimation of N_C would result in a negative shift of E_{CB} relative to E_{FB} (eq 1). However, an unrealistically large N_C value of 10^{37} cm^{-3} would be implied if E_{CB} was shifted far enough negative to account for the photocurrent maximum at pH 4 for **1**-derivatized TiO_2. The overlap of pH dependencies for low-surface-area and nanocrystalline TiO_2 also suggests that a large difference between E_{CB} and E_{FB} is unlikely to account for the data, because nanocrystalline TiO_2 is incapable of supporting a significant space charge layer.[55] Furthermore, the plots of photocurrent vs pH for different porphyrins would still be displaced along the pH axis, regardless of the separation between E_{CB} and E_{FB}. Finally, we have considered the possibility that electron injection occurs by the reduction of a discrete TiO_2 surface state at higher energy than the conduction band. While this mechanism would account for the shifts of photocurrent onsets to more acidic pH's than expected, it still would not account for the sensitizer-independent photocurrent vs pH data.

SCHEME 1: Mechanism of pH-dependent Charge Collection Efficiency. (a) Basic pH, Electron Injection Is Followed by Rapid Charge Recombination. (b) Acidic pH, Electron Injection Is Followed by Transport through the Film. Proton Intercalation May Accompany Electron Transport

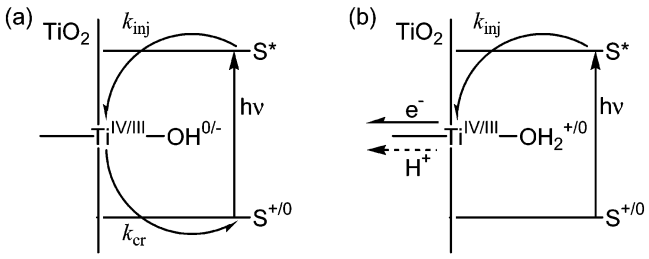

Based on the arguments outlined above, we have concluded that the dependence of sensitized photocurrent on electrolyte pH cannot be accounted for by pH-dependent electron injection yields. We instead attribute the effect to pH-dependent charge collection efficiency (η_{el}). The photoelectrochemical and spectroscopic data imply that η_{el} increases with decreasing pH. We attribute the pH dependence of η_{el} to the influence of surface protonation-deprotonation equilibria on charge compensation of the injected electron. In the proposed mechanism outlined in Scheme 1, protonation of a surface site is required for charge compensation of injected electrons. At basic pH's, where deprotonated $Ti^{IV}-OH$ surface sites predominate, electron injection is followed by rapid charge recombination to the oxidized porphyrin. At acidic pH's, where protonated $Ti^{IV}-OH_2^+$ surface sites predominate, the injected electrons are stabilized by the positive charge on the TiO_2 surface. Efficient charge compensation enables the transport of electrons through the TiO_2 film to the back contact of the working electrode. Our photoelectrochemical and spectroscopic data do not allow us to determine whether the protonated $Ti^{IV}-OH_2^+$ surface state is reduced directly by the sensitizer excited-state or by a conduction band electron following injection.

In light of the proposed mechanism, the plots of photocurrent vs pH (Figure 4a, inset) or $\Delta A_0/\Delta A_{0,max}$ vs pH (Figure 7) represent Bronsted acid−base titrations of surface sites. The midpoints of the sensitized photocurrent onsets and transient absorbance onsets correspond to the pK_{a1} of $Ti^{IV}-OH_2^+$ sites. The midpoints occurred from pH 6 to 6.5, which is in reasonable agreement with the pK_{a1} value of 5.0 reported by Schindler and Gamsjäger[62] and the isoelectronic point of 5 reported by McQuillan et al.[63,64] Sensitized photocurrents and transient absorbances were maximized below pH 5, where the surface is positively charged.

For this mechanism to be correct and consistent with experimental data, electron injection and charge recombination must occur within our transient absorption instrument response time. At basic pH's, no evidence for electron injection or charge recombination was seen, implying that $k_{inj} > 10^8\ s^{-1}$ and $k_{cr} > 10^8\ s^{-1}$. Lian and co-workers[65−68] have recently reported rapid nonexponential charge recombination for dye-sensitized nanocrystalline TiO_2 with ≥70% of recombination occurring in less than 1 ns. Similarly, Willig et al.[69] reported nonexponential recombination that was completed in less than 1.5 ns.

Our proposed mechanism is also consistent with Lyon and Hupp's[70,71] observation that electrochemical reduction of nanocrystalline TiO_2 films is accompanied by reversible proton uptake from aqueous solution. They have attributed the proton uptake to adsorption or intercalation driven by charge compensation of conduction band electron density. We speculate that proton intercalation may be coupled to electron transport at acidic pH's. However, our photoelectrochemical and spectroscopic measurements do not enable us to directly probe the concentration of protons within the TiO_2 film.

The dependence of charge collection efficiency on electrolyte pH affects the energetic requirements for maximizing the global efficiency of dye-sensitized photoelectrochemical cells. The global efficiency is proportional to the short circuit photocurrent and the open circuit voltage. The short circuit photocurrent depends on ϕ_{inj} and η_{el} (eq 2). For both ϕ_{inj} and η_{el} to be simultaneously maximized, the entire excited-state distribution function ($W_{don}(E)$) must lie at more negative potential than E_{CB} at electrolyte proton concentrations sufficient for charge compensation of the injected electron. Open circuit voltage is maximized when $W_{don}(E)$ is only minimally more negative than E_{CB}. It is often assumed that the pH dependence of E_{CB} should enable some tunability of the open circuit voltage without affecting the short circuit photocurrent. However, the pH dependence of charge collection efficiency implies that this is not the case. The interplay between maximizing open circuit voltage and short circuit photocurrent imparts specific energetic requirements on the choices of semiconductor, sensitizer, and electrolyte composition. For example, the porphyrin sensitizers employed in this study are not ideal for maximizing the global efficiency of aqueous dye-sensitized TiO_2 cells. At acidic pH's, where maximum photocurrents were measured, $E_{1/2}(P^{+/*})$ values for **1**−**4** ranged from 1.1 to 1.6 eV negative of E_{CB}. Electron injection is unnecessarily exergonic, resulting in unrecoverable losses of energy upon electron injection. However, raising the pH to minimize the free energy lost in the injection process fails, as this provides insufficient proton concentration for efficient charge collection.

Conclusions

We have reported pH-dependent photocurrents and transient absorption data for porphyrin-sensitized TiO_2. Sensitized photocurrents were "turned off" at electrolyte pH's above 10, even though electron injection was thermodynamically favored. Plots of photocurrent vs pH and $\Delta A_0/\Delta A_{0,max}$ vs pH were independent of the porphyrin used, despite the 670 mV range of $E_{1/2}(P^{+/*})$ values for **1**−**4**. Identical pH-dependencies were observed for low-surface-area and nanocrystalline TiO_2. The data indicate that the charge collection efficiency, and not the electron injection yield, is pH-dependent. We have proposed a mechanism in which trapping of the injected electron at Ti^{IV}-OH_2^+ surface sites leads to efficient charge collection, while trapping at Ti^{IV}-OH sites leads to efficient charge recombination. Thus, the charge collection efficiency is determined by surface protonation-deprotonation equilibria. Our findings have implications with regard to the design of efficient dye-sensitized photoelectrochemical cells. Judicious choices of semiconductor, sensitizer, and electrolyte are required to maximize the open circuit voltage while simultaneously optimizing the electron injection and charge collection efficiencies.

Acknowledgment. The porphyrin complexes **1**, **2**, and **4** were provided by Mr. W. J. Youngblood, Dr. K. Muthukumaran, and Prof. J. S. Lindsey. We thank Profs. Lindsey, D. Holten, and D. Bocian for helpful discussions. This research was funded by the National Renewable Energy Laboratory.

References and Notes

(1) Gerischer, H. *Photochem. Photobiol.* **1972**, *16*, 243−260.
(2) Memming, R. *Photochem. Photobiol.* **1972**, *16*, 325−333.
(3) Hagfeldt, A.; Grätzel, M. *Chem. Rev.* **1995**, *95*, 49−68.
(4) Kalyanasundaram, K.; Grätzel, M. *Coord. Chem. Rev.* **1998**, *77*, 347−414.
(5) Qu, P.; Meyer, G. J. In *Electron Transfer in Chemistry*; Balzani, V., Ed.; John Wiley and Sons: New York, 2001; Vol. IV, pp 355−411.
(6) Gerischer, H. *Surf. Sci.* **1969**, *18*, 97−122.
(7) Gleria, M.; Memming, R. *Z. Phys. Chem. (Munich)* **1975**, *98*, 303−316.
(8) Memming, R. *Surf. Sci.* **1980**, *101*, 551−563.
(9) Desilvestro, J.; Grätzel, M.; Kavan, L.; Moser, J. *J. Am. Chem. Soc.* **1985**, *107*, 2988−2990.
(10) Kalyanasundaram, K.; Vlachopoulos, N.; Krishnan, V.; Monnier, A.; Grätzel, M. *J. Phys. Chem.* **1987**, *91*, 2342−2347.
(11) Vlachopoulos, N.; Liska, P.; Augustynski, J.; Grätzel, M. *J. Am. Chem. Soc.* **1988**, *110*, 1216−1220.
(12) Liska, P.; Vlachopoulos, N.; Nazeeruddin, M. K.; Comte, P.; Grätzel, M. *J. Am. Chem. Soc.* **1988**, *110*, 3686−3687.
(13) O'Regan, B.; Grätzel, M. *Nature* **1991**, *353*, 737−740.
(14) Nazeeruddin, M. K.; Kay, A.; Rodicio, I.; Humphry-Baker, R.; Müller, E.; Liska, P.; Vlachopoulos, N.; Grätzel, M. *J. Am. Chem. Soc.* **1993**, *115*, 6382−6390.
(15) Grätzel, M. In *Future Generation Photovoltaic Technologies: AIP Conference Proceedings*; McConnell, R. D., Ed.; NREL: Denver, CO, 1997.
(16) Watson, D. F.; Meyer, G. J. *Coord. Chem. Rev.* In press.
(17) Finklea, H. O. In *Semiconductor Electrodes*; Finklea, H. O., Ed.; Elsevier: New York, 1988; pp 43−145.
(18) Watanabe, T.; Fujishima, A.; Honda, K. *Bull. Chem. Soc. Jpn.* **1976**, *49*, 355−358.
(19) Bolts, J. M.; Wrighton, M. S. *J. Phys. Chem.* **1976**, *80*, 2641−2645.
(20) Rothenberger, G.; Fitzmaurice, D.; Grätzel, M. *J. Phys. Chem.* **1992**, *96*, 5983−5986.
(21) Redmond, G.; Fitzmaurice, D. *J. Phys. Chem.* **1993**, *97*, 1426−1430.
(22) Boschloo, G.; Fitzmaurice, D. *J. Phys. Chem. B* **1999**, *103*, 7860−7868.
(23) Liu, Y.; Hagfeldt, A.; Xiao, X.-R.; Lindquist, S.-E. *Sol. Energy Mater.* **1998**, *55*, 267−281.
(24) Kelly, C. A.; Farzad, F.; Thompson, D. W.; Stipkala, J. M.; Meyer, G. J. *Langmuir* **1999**, *15*, 7047−7054.
(25) Tachibana, Y.; Haque, S. A.; Mercer, I. P.; Moser, J. E.; Klug, D. R.; Durrant, J. R. *J. Phys. Chem. B* **2001**, *105*, 7424−7431.
(26) Asbury, J. B.; Anderson, N. A.; Hao, E.; Ai, X.; Lian, T. *J. Phys. Chem. B* **2003**, *107*, 7376−7386.
(27) Kopidakis, N.; Schiff, E. A.; Park, N.-G.; van de Lagemaat, J.; Frank, A. J. *J. Phys. Chem. B* **2000**, *104*, 3930−3936.
(28) Kambe, S.; Nakade, S.; Kitamura, T.; Wada, K.; Yanagida, S. *J. Phys. Chem. B* **2002**, *106*, 2967−2972.
(29) Watanabe, T.; Fujishima, A.; Tatsuoki, O.; Honda, K.-i. *Bull. Chem. Soc. Jpn.* **1976**, *49*, 8−11.
(30) Clark, W. D. K.; Sutin, N. *J. Am. Chem. Soc.* **1977**, *99*, 4676−4682.
(31) Sonntag, L. P.; Spitler, M. T. *J. Phys. Chem.* **1985**, *89*, 1453−1457.
(32) Watson, D. F.; Marton, A.; Stux, A. M.; Meyer, G. J. *J. Phys. Chem. B* **2003**, *107*, 10971−10973.
(33) Lindsey, J. S.; Prathapan, S.; Johnson, T. E.; Wagner, R. W. *Tetrahedron* **1994**, *50*, 8941−8968.
(34) Muthukumaran, K.; Loewe, R. S.; Ambroise, A.; Tamaru, S.-i.; Li, Q.; Mathur, G.; Bocian, D. F.; Misra, V.; Lindsey, J. S. *J. Org. Chem.* **2004**, *69*, 1444−1452.
(35) Mink, L. M.; Neitzel, M. L.; Bellomy, L. M.; Falvo, R. E.; Boggess, R. K.; Trainum, B. T.; Yeaman, P. *Polyhedron* **1997**, *16*, 2809−2817.

(36) Ting, C.-C.; Chen, S.-Y.; Liu, D.-M. *J. Appl. Phys.* **2000**, *88*, 4628−4633.
(37) Ting, C.-C.; Chen, S.-Y.; Liu, D.-M. *Thin Solid Films* **2002**, *402*, 290−295.
(38) Heimer, T. A.; D'Arcangelis, S. T.; Farzad, F.; Stipkala, J. M.; Meyer, G. J. *Inorg. Chem.* **1996**, *35*, 5319−5324.
(39) Bonhôte, P.; Gogniat, E.; Tingry, S.; Barbé, C.; Vlachopoulos, N.; Lenzmann, F.; Comte, P.; Grätzel, M. *J. Phys. Chem. B* **1998**, *102*, 1498−1507.
(40) Langmuir, I. *J. Am. Chem. Soc.* **1918**, *40*, 1361−1402.
(41) Kynukshto, V. N.; Solovyov, K. N.; Egorova, G. D. *Biospectroscopy* **1998**, *4*, 121−133.
(42) Chirvony, V. S.; van Hoek, A.; Galievsky, V. A.; Sazanovich, I. V.; Schaafsma, T. J.; Holten, D. *J. Phys. Chem. B* **2000**, *104*, 9909−9917.
(43) Mott, N. F. *Proc. R. Soc. London, Ser. A* **1939**, *171*, 27.
(44) Schottky, W. *Z. Phys.* **1942**, *118*, 539−592.
(45) Gomes, W. P.; Cardon, F. *Z. Phys. Chem. (Munich)* **1973**, *86*, 330−334.
(46) Frank, S. N.; Bard, A. J. *J. Am. Chem. Soc.* **1975**, *97*, 7427−7433.
(47) Zaban, A.; Ferrere, S.; Gregg, B. A. *J. Phys. Chem. B* **1998**, *102*, 452−460.
(48) Tokel-Takvoryan, N. E.; Bard, A. J. *Chem. Phys. Lett.* **1974**, *25*, 235−238.
(49) Rehm, D.; Weller, A. *Isr. J. Chem.* **1970**, *8*, 259−271.
(50) Bailey, S. I.; Ritchie, I. M.; Hewgill, F. R. *J. Chem. Soc., Perkin Trans. 2* **1983**, 645−653.
(51) Södergren, S.; Hagfeldt, A.; Olsson, J.; Lindquist, S.-E. *J. Phys. Chem.* **1994**, *98*, 5552−5556.
(52) Rodriguez, J.; Kirmaier, C.; Holten, D. *J. Am. Chem. Soc.* **1989**, *111*, 6500−6506.
(53) Pekkarinen, L.; Linschitz, H. *J. Am. Chem. Soc.* **1960**, *82*, 2407−2411.
(54) Felton, R. H. In *The Porphyrins*; Dolphin, D., Ed.; Academic Press: New York, 1978; Vol. 5, pp 53−125.
(55) Albery, W. J.; Bartlett, P. N. *J. Electrochem. Soc.* **1984**, *131*, 316−325.
(56) Finklea, H. O. In *Semiconductor Electrodes*; Finklea, H. O., Ed.; Elsevier: New York, 1988; pp 1−42.
(57) Watanabe, T.; Fujishima, A.; Honda, K.-I. *Chem. Lett.* **1974**, 897−900.
(58) Nozik, A. J. *Annu. Rev. Phys. Chem.* **1978**, *29*, 189−222.
(59) Gerischer, H. In *Physical Chemistry: An Advanced Treatise*; Eyring, H., Henderson, D., Jost, W., Eds.; Academic Press: New York, 1970; Vol. 9A, pp 463−542.
(60) Stanienda, A.; Bieble, G. *Z. Phys. Chem. (Munich)* **1967**, *52*, 254−275.
(61) Giraudeau, A.; Callot, H. J.; Gross, M. *Inorg. Chem.* **1979**, *18*, 201−206.
(62) Schindler, P. W.; Gamsjäger, H. *Discuss. Faraday Soc.* **1971**, *52*, 286−288.
(63) Dobson, K. D.; Connor, P. A.; McQuillan, A. J. *Langmuir* **1997**, *13*, 2614−2616.
(64) Connor, P. A.; Dobson, K. D.; McQuillan, A. J. *Langmuir* **1999**, *15*, 2402−2408.
(65) Ghosh, H. N.; Asbury, J. B.; Weng, Y.; Lian, T. *J. Phys. Chem. B* **1998**, *102*, 10208−10215.
(66) Weng, Y.; Wang, Y.-Q.; Asbury, J. B.; Ghosh, H. N.; Lian, T. *J. Phys. Chem. B* **2000**, *104*, 93−104.
(67) Hao, E.; Anderson, N. A.; Asbury, J. B.; Lian, T. *J. Phys. Chem. B* **2002**, *106*, 10191−10198.
(68) Wang, Y.; Hang, K.; Anderson, N. A.; Lian, T. *J. Phys. Chem. B* **2003**, *107*, 9434−9440.
(69) Hannappel, T.; Burfeindt, B.; Storck, W.; Willig, F. *J. Phys. Chem. B* **1997**, *101*, 6799−6802.
(70) Lyon, L. A.; Hupp, J. T. *J. Phys. Chem.* **1995**, *99*, 15718−15720.
(71) Lyon, L. A.; Hupp, J. T. *J. Phys. Chem. B* **1999**, *103*, 4623−4628.